



# Research on Laser Thread Form Bending of Stainless Steel Tube

Fuqiang Li<sup>1</sup> · Shourong Liu<sup>2</sup> · Aiping Shi<sup>1</sup> · Qiulu Chu<sup>1</sup> · Qiang Shi<sup>1</sup> · Yuxiang Li<sup>1</sup>

Received: 16 April 2018 / Revised: 2 November 2018 / Accepted: 18 November 2018 / Published online: 24 April 2019  
© Korean Society for Precision Engineering 2019

## Abstract

Compared to traditional bending methods, laser bending can yield products with better shapes and higher quality using the simpler equipment. In this paper, the mechanism of Laser-assisted tube bending is elaborated, and then the influence of processing parameters (including laser power, scanning speed, spot diameter, and scanning times) on the bending angle is studied with both the finite element method and experiments. The bending angle increases with an increase of laser power and spot diameter and with a decrease in the scanning speed. Three-dimensional (3D) thread form bending can be achieved by planning the optimal route, scanning parameters, and the number of laser scans. In contrast to the desired thread diameter of 20 mm and thread pitch of 180 mm, the resulting thread of the stainless steel tube is close to the target shape with errors of 3% for thread diameter and 2.5% for thread pitch, which are both in an acceptable range and thus verify the validity of the parameters selection and route planning method.

**Keywords** Stainless steel tube · Laser · Thread form bending · Path planning

## 1 Introduction

Because of the advantages of lightweight and shock absorption effectiveness, tubular parts have been widely used to manufacture various parts and applied in many fields, such as the auto industry, aerospace manufacturing, shipbuilding industry, and light industry [1–3].

Traditional bending methods of tube stock include die bending, roll bending, push bending, stretch bending, rotary bending, and so on [4]. However, there are flaws with these technologies, such as spring back, wrinkling, thinning damage, cross-section deformation, etc. [5]. Laser bending can effectively avoid these shortcomings because of its forming mechanism of inner heterogeneous thermal stresses induced by laser beam irradiation. There are many advantages to the laser bending method: high bending precision, no spring back, fitting for thin-walled tubes, accurately controlled heat source, and good environmental adaptability [6]. Therefore, it is widely used in the bending process of many

metal materials. Laser bending is especially suitable for thin-walled or hard material tubes that cannot be finished with traditional methods. It can replace traditional bending technology in a number of situations [7].

The mechanism and application of laser bending of tube have been studied for many years. Silve et al. and Kraus investigated laser bending of square cross-section tube using experimental and FEM method respectively [8, 9]. Bending angles and variation in thickness were all well studied, as well as the plastic deformation mechanism. Li et al. explained the causes of deformation characteristics such as wall thickness variation, protruded intrados, and bending radius in detail [10]. Hao and Li established a new analytical model to describe the relationships between the bending angle and the processing parameters, including the laser energy, geometric and material properties [11, 12]. Safdar thought deeply on the dissimilar of the canning schemes between beam geometries with rectangular beam used for the axial scanning and circular beam for circumferential scan [13]. Three scanning schemes (alternate circumferential, axial and sequential circumferential) were modelled to investigate the effect of scanning direction on circular laser tube bending.

The above researches focused on the laser bending mechanism of tube using different methods. In recent years, more studies were conducted to achieve accuracy control of 3D

✉ Aiping Shi  
aiping\_shi@yeah.net

<sup>1</sup> School of Agricultural Equipment Engineering, Jiangsu University, 301, Xuefu Road, Zhenjiang 212013, China

<sup>2</sup> College of Engineering, China Agricultural University, 17, Tsinghua East Road, Haidian, Beijing 100083, China

laser forming of the tube. Guan et al. constructed a 3D thermomechanical finite element model to analyze laser tube bending precisely [14]. They integrated the finite element simulation with genetic algorithm, which optimized the laser bending process of tubes. Wang presented a bending strategy for laser bending of a straight tube into a curved tube and carried out an experiment to verify its validity [15, 16]. Imhan, from University Putra Malaysia, researched the laser bending of stainless steel 304 tubes via irradiation by an Nd-YAC laser [17–19]. An analytical model was established to analyze the effects of laser power and scanning speed on the bending angle of the tube and verified experimentally.

In practical work of laser tube bending, it is important to select proper processing parameters according to the target form of the product, including laser power, scanning speed, scanning route, scanning times, and so on. However, it is not always clear how to do so. In this paper, an indirect coupling analysis method is used to simulate the bending process under laser irradiation with different parameters, aiming to find out the relationship of bending angle with each process parameter. Furthermore, a path planning strategy for thread form bending of tubes is proposed. The strategy containing planning the optimal route, scanning steps, scanning times and process parameters to obtain the target thread shape.

## 2 Materials and Methods

### 2.1 Principle of Laser Bending

Laser bending of a tube is a kind of thermal stress forming. Temperature gradient mechanism and upsetting mechanism are used in the forming process.

The mechanisms are reflected in the two stages of the bending process: a warming stage and a cooling stage.

During the warming stage, the tube obtains uneven thermal stress distribution when the laser beam is applied to the tube. When the thermal stress exceeds the yield limit of the material, the tube is compressed along the axial direction, resulting in the thickening of the tube wall [12].

The cooling stage begins with the shutdown of the laser beam, followed by a rapid drop in temperature of the irradiated side. Because of the uneven thermal distribution, the temperature of the irradiated side drops faster than the other side. Thus, the shrinkage degree of the irradiated side is higher than the other side, leading to the bending of the tube faced to the irradiated side.

The bending angle of the tube is affected by four types of parameters: thermophysical and mechanical properties of the material, geometrical parameters of the tube, optical parameters of the laser, and technological parameters of the process. Once the material and dimensions of the tube are determined, the predominant parameters are laser power,

scanning speed, scanning wrap angle, spot diameter, and scanning time.

### 2.2 Simulation Method Based on Finite Element

The bending of the tube under laser scanning is a thermal-structural coupling process. An indirect coupling analysis method can be used to analyze the tube laser forming by solving every physical field model with specific order. In this analysis process, the former solving result is taken as the load and boundary condition for the following step. Taking ANSYS as the analysis platform, APDL language was used to program the coupling method and achieve the analysis of temperature field, stress field, and displacement field. The finite element analysis process in ANSYS is expressed in Fig. 1.

#### 2.2.1 Performance Parameters of Material

The material analyzed in this paper is AISI 304L stainless steel, whose chemical composition and physical parameters are shown in Table 1. According to Peckner and Bernstein, the parameters of the thermophysical characteristics and mechanical properties of a material are relevant to the temperature of that material [20]. The relationships of typical properties with temperature are shown in Fig. 2.

#### 2.2.2 Elements Selection and Meshing

The two stages in the process of indirect coupling analysis shown in Fig. 1 each need their own element. Element SOLID70 was used for 3D thermal analysis of both the steady state and transient state, while element SOLID45 was suitable for the structural analysis of stainless steel. The two elements can meet the computing needs for the analysis.

Considering both computational accuracy and computational scale in the process of simulation, meshing is very important. The gridding near the laser scanning track was dense to ensure the computational accuracy, while the gridding far away from the laser scanning track was sparse to shorten the computing time, as shown in Fig. 4. There were 6300 nodes and 4800 elements in the model with dimensions of 10 mm × 1 mm × 50 mm (outer diameter × wall thickness × tube length).

#### 2.2.3 Boundary Conditions Definition

The initial temperature of the tube was set as room temperature (20 °C). One end of the tube was fixed with a chuck while the other was free.

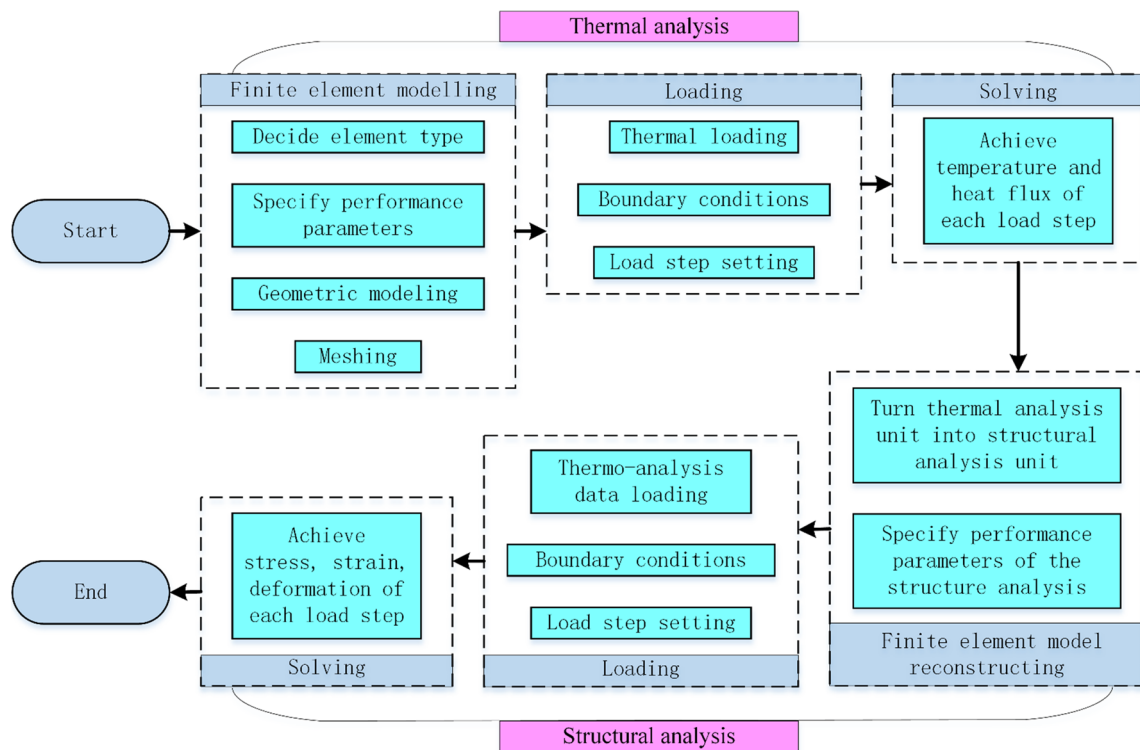


Fig. 1 Flow chart of finite element analysis for laser tube bending

Table 1 Chemical composition and physical parameters of AISI 304L stainless steel

Chemical composition (%)							Physical parameters		
C	Si	Mn	Cr	Ni	S	P	Density (kg/m <sup>3</sup> )	Melting point (K)	Poisson's ratio
≤0.03	≤1.00	≤2.00	18–22	9–13	≤0.03	≤0.045	7854	1751	0.3

2.2.4 Thermal Loading

The light spot formed due to the irradiation of the tube surface by the laser beam can be taken as a circular moving heat source with Gaussian distribution, which is transferred to square spot with the dimension of  $l \times l$  mm<sup>2</sup> to simplify the calculation [14]. The circular heat source was simplified to a square light spot with average heat flux density of  $I_m$ .

The heat flux density of the Gaussian distribution was [14]

$$I = \frac{2AP}{\pi r_b^2} \exp\left(-\frac{2r^2}{r_b^2}\right), \tag{1}$$

where  $A$  is the absorption coefficient,  $P$  is the laser output power,  $r_b$  is the radius of the laser beam irradiated to the surface of the tube, and  $r$  is the distance between the observed point and the laser beam center.

The distribution of  $I$  can be expressed as Fig. 3.

In Fig. 3,  $x$ - $y$  plane scanning surface of the laser spot with a certain radius of  $r_b$ ,  $r^2 = (x - x_{centre})^2 + (y - y_{centre})^2$ , Energy( $AP$ ) means the heat flux density of different point inside of the laser spot.

The average heat flux density within the laser beam range was [14]

$$I_m = \frac{1}{\pi r_b^2} \int_0^{r_b} I(2\pi r) dr \tag{2}$$

$$= \frac{2\pi}{\pi r_b^2} \int_0^{r_b} \frac{2AP}{\pi r_b^2} \exp\left(-\frac{2r^2}{r_b^2}\right) r dr = \frac{0.865AP}{\pi r_b^2},$$

where  $A$ ,  $P$ ,  $r_b$ , and  $r$  as specified above.

The above average heat flux density  $I_m$  was used as the thermal load in the finite element model, as shown in Fig. 4. The irradiation points and scanning direction are shown in Fig. 5. Points 1–3 present the route of one scan. Point 4 and point 5 are the inner surfaces of the tube, while points 5 and 6 are at the unscanned side of the tube. The laser beam scans circumferentially with constant speed,

**Fig. 2** Variation law of properties (specific heat capacity, thermal expansion coefficient, thermal conductivity, elasticity modulus and yield strength) of AISI 304L stainless steel with temperature change

dividing into 23 loading steps [7]. The process parameters in the simulation are shown in Table 2.

### 2.3 Experiment Material and Equipment

The experiment was carried out with a numerical control laser scanning test bench and a CO<sub>2</sub> laser with maximum continuous output power of 3 kW. The material of the tube specimen was AISI 304L stainless steel, with dimensions of 10 mm × 1 mm × 50 mm (outer diameter × wall thickness × tube length). One end of the tube specimen was installed on the chuck and the other was free. The chuck was fixed on a NC table, which allowed the rotating and moving of the tube to adjust the proper scanning position. After the laser bending and cooling stage were complete, a micrometer was used to measure the displacement of the free end [5, 10]. A diagrammatic sketch and a photograph of the layout of the experiment equipment setup are shown in Fig. 6.

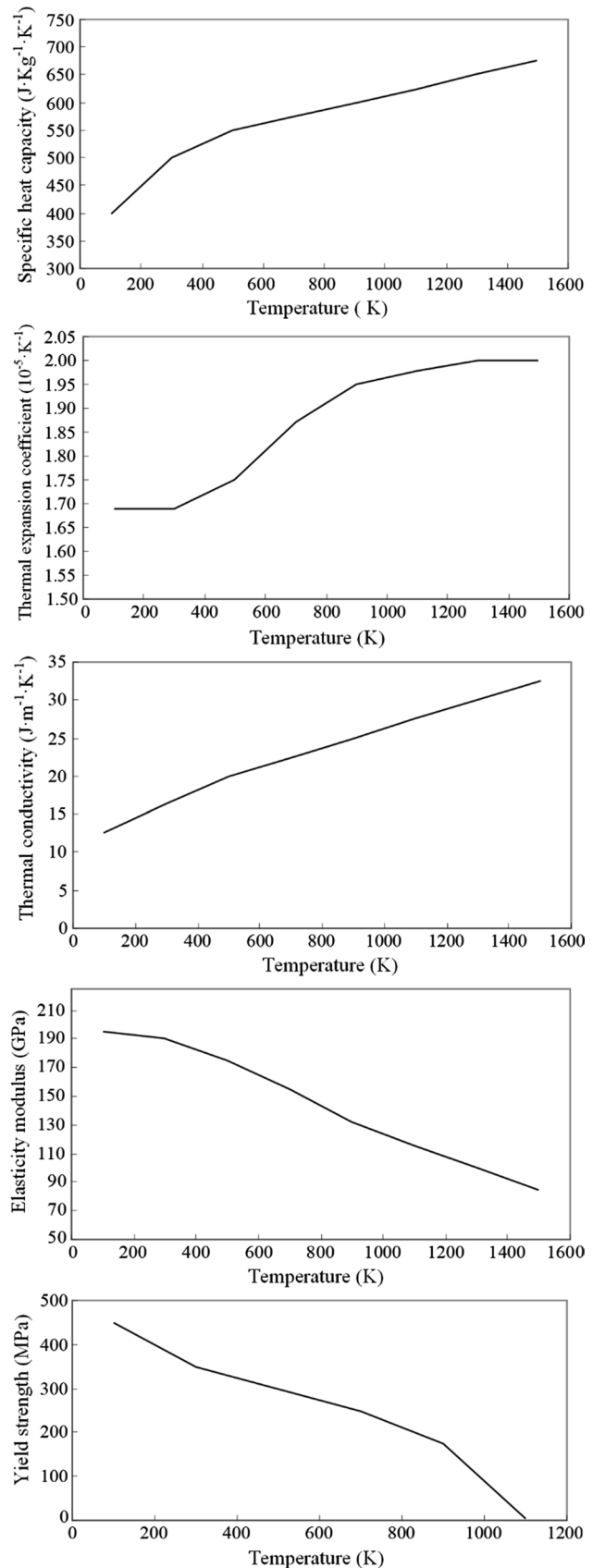
Through a series of tests under different conditions, the relationships of the processing parameters (laser power, rotationscanning speed, spot diameter, and scanning numbers) with bending angle of the tube were determined, which laid the groundwork for the subsequent path planning strategy of thread form bending.

### 2.4 Path Planning Strategy for Laser Thread Form Bending

Any complex three-dimensional bending of a tube can be seen as the combination of one-direction bending of points along its axis. Thus, 3D bending of a tube can be achieved by choosing the bending position and direction in each step of one-direction bending [21]. Thread form bending is a special case of 3D continuous bending of the tube, which can be achieved with correct path planning, scanning direction, and processing parameters.

First, the target thread form tube is simplified to be a thread line along its axis. Then the thread line is divided into *N* sections and each section can be approximated as 2D bending of the tube in a plane.

The bending angle of each section of the tube can be obtained by calculating the relative coordinates of points at its two ends. According to the bending angle and size of the tube, a group of appropriate processing parameters is selected. All the sections share the same processing parameters and bending shape due to equal division of the tube. Each section bends on the basis of the previous section and



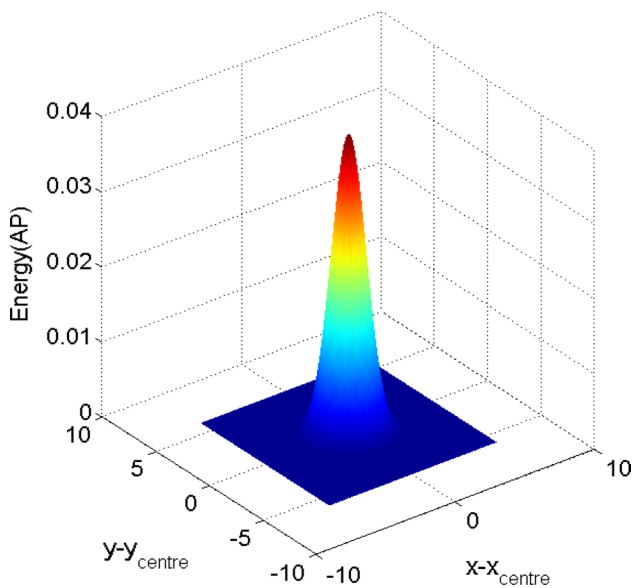


Fig. 3 Distribution of the heat flux density ( $r_b = 2\text{ mm}$ )

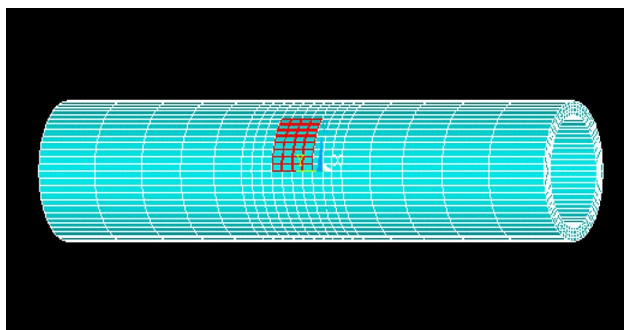


Fig. 4 Finite element model after meshing and loading

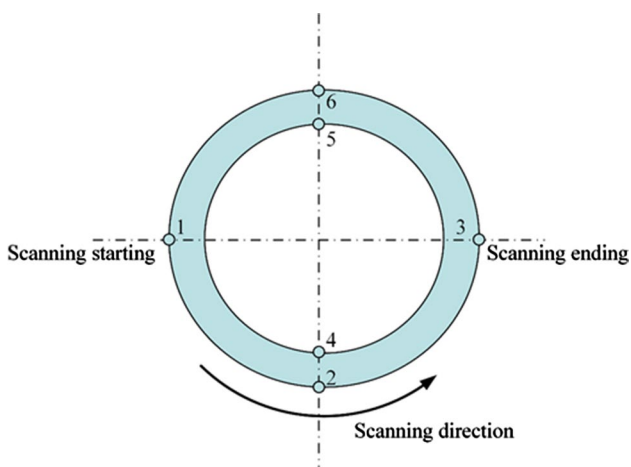
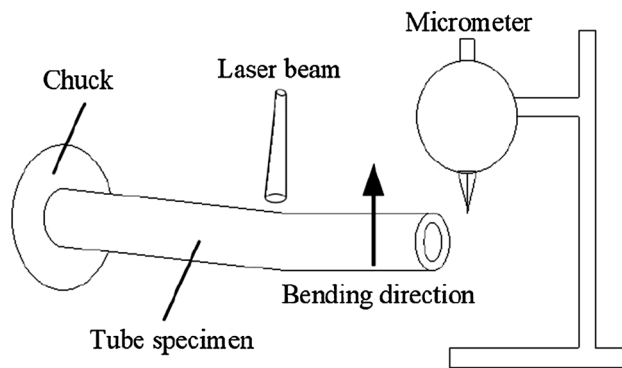


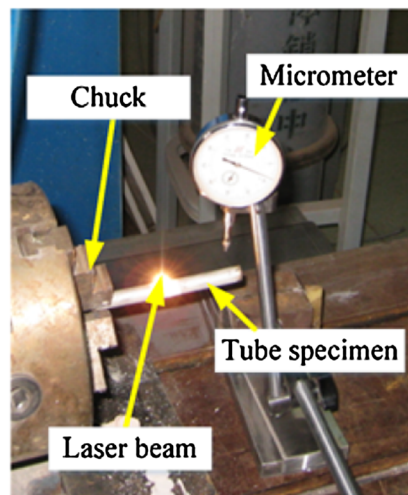
Fig. 5 The scanning direction in simulation of laser tube bending [7]

Table 2 Process parameters in the simulation

Process parameters	Value
Laser power	600 W
Wrap angle	180°
Scanning speed	20 mm/s
Spot dimension	4×4 mm <sup>2</sup>
Absorption coefficient	0.5



(a) Diagrammatic sketch of the experiment idea <sup>10</sup>



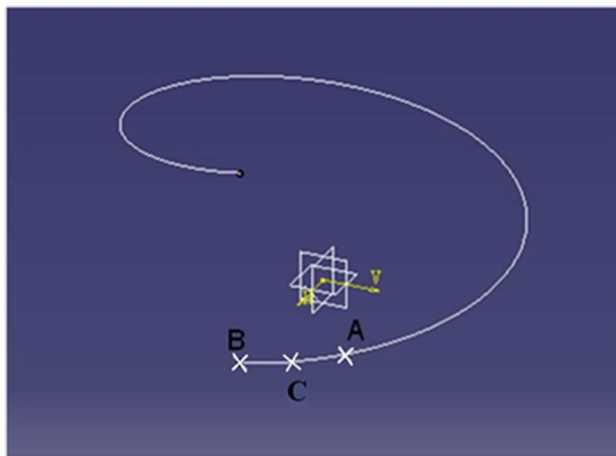
(b) Experiment photo

Fig. 6 Laser scanning experiment

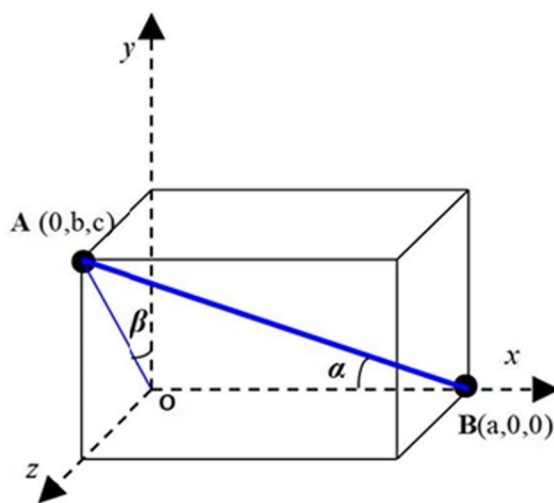
the bending accumulate until a thread-like tube is produced [16].

Taking a few sections from the N divided sections as an example, path planning of the thread form bending of the tube can be explained.

As shown in Fig. 7a, points A and B are the two ends of the tube axis section, while C is the middle point. The line A–C–B is the axis of the bending tube. According to the radius and thread pitch of the screw thread, the coordinates of points A and B can be ascertained, as shown in Fig. 7b. The angle  $\angle\alpha$  is the desired one-direction bending angle of the A–B section,



(a) Points on the tube axis



(b) Coordinates of points A and B

Fig. 7 Position of A, B and C

which can be calculated from the geometrical relationship of points A and B. There was an angle of  $\beta$  between plane  $xy$  and plane  $AOB$  that contained the bending section of the tube. Because the direction of the laser beam is required to be perpendicular with plane  $AOB$ , the circumferential deviation angle between the adjacent scanning trajectories was identified as  $\beta$ .

In accord with Fig. 7b, the coordinates of A and B are expressed as  $A(0, b, c)$  and  $B(a, 0, 0)$ . The formulas for calculating  $a$ ,  $b$ ,  $c$ ,  $\alpha$ , and  $\beta$  are shown below [16]:

$$a = \frac{P}{n}, \quad (3)$$

$$b = \frac{D}{2} \sin\left(\frac{360^\circ}{n}\right), \quad (4)$$

$$c = \frac{D}{2} - \frac{D}{2} \cos\left(\frac{360^\circ}{n}\right), \quad (5)$$

$$\alpha = \arctan\left(\frac{\sqrt{b^2 + c^2}}{a}\right), \quad (6)$$

$$\beta = \arctan\left(\frac{c}{b}\right), \quad (7)$$

where  $P$  is the pitch,  $n$  is the number of segments in one circle of thread,  $D$  is the outer diameter of the thread,  $\alpha$  is the desired one-direction bending angle the tube, and  $\beta$  is the circumferential angle between adjacent scanning trajectories.

Finally, we chose the processing parameters including laser power, spot diameter, and scanning speed according to the relationships of these variables with bending angle, which were determined in the former experiments. Then we determined the scanning time needed to achieve the bending angle  $\alpha$  based on the relation of the scanning time with the bending angle.

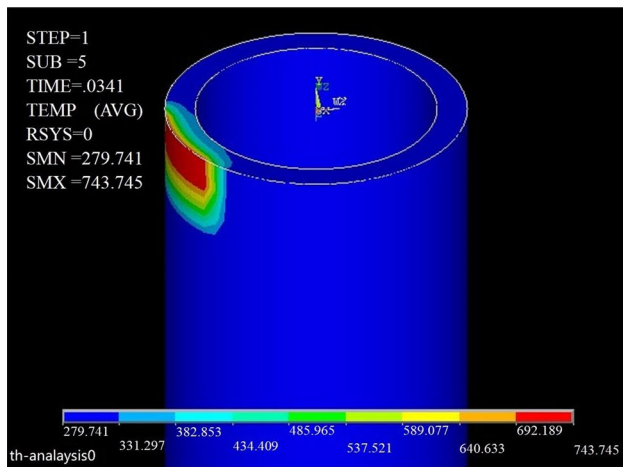
Because the tube bends after being scanned by the laser, the scan should start from the free end and scan along the trajectories one by one. Each trajectory must be scanned a certain number of times to achieve the desired bending angle. After the completion of one trajectory, the tube was rotated along the scanning direction by an angle of  $\beta$  degrees and moving to the right position. Then, the next trajectory was scanned with the same processing parameters until the last trajectory was finished.

## 3 Results and Discussions

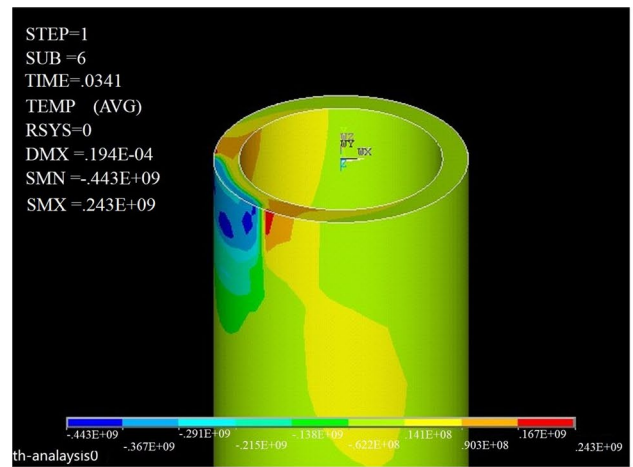
### 3.1 Results of Finite Element Analysis

#### 3.1.1 Temperature Field Analysis Results

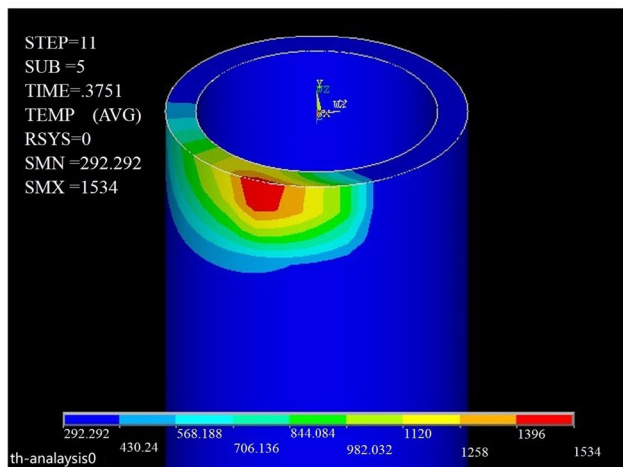
It can be seen from Fig. 8 that in the laser spot acting area at the starting point, the temperature of the material surface changed rapidly and there were obvious temperature gradients between the internal and external surface, which accord with the temperature gradient mechanism. The inner surface temperature rapidly rose to 383 K in 0.0341 s. As scanning proceeded, the temperature of the scanned areas gradually reduced, while the temperatures of ready-to-be-scanned areas rapidly increased due to heat conduction. The temperature gradient of the scanned area was mainly in the circular direction of the tube, while the



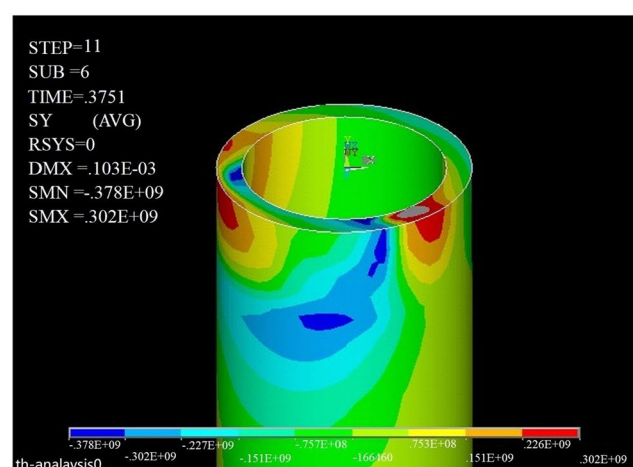
(a) Starting point



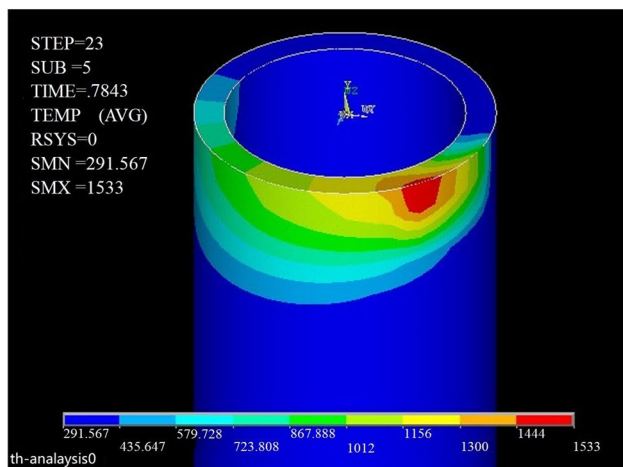
(a) Starting point



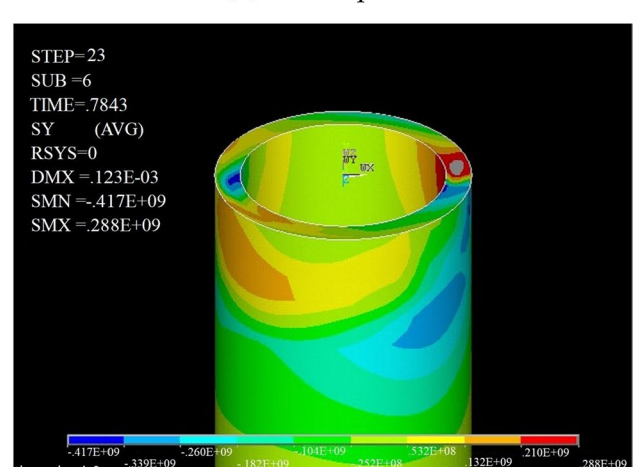
(b) Middle point



(b) Middle point



(c) Ending point



(c) Ending point

Fig. 8 Thermal distribution at three typical stages

Fig. 9 Stress distribution at three typical stages

temperature gradient of the ready-to-be-scanned area was still in the wall thickness direction until the irradiation is finished. In the process of scanning, the highest temperature reached 1534 K, which is lower than the melting point of the material.

### 3.1.2 Stress Field Analysis Results

As shown in Fig. 9, at the starting point of heating, the material temperature in the area of light spot radiation increased rapidly, which caused the material to expand. However, the expanding material was bound by the cold material around it, causing compression stress. Because the temperature of the outer surface was the highest, the resulting axial stress and strain was relatively larger. With the temperature increased, larger axial expansion was produced at the area of light spot radiation, which led to the increase of compression stress and compression strain. After cooling off, the axial stress of the scanning area was composed of compression stress in the outer surface and tensile stress in the inner surface.

### 3.1.3 Deformation and Bending Angle in Simulation

With the irradiation of the laser beam, the free end of the tube was displaced to the backward direction of the laser beam because of the rising temperature and expansion of the heating area. After the tube cooled off, the state of the heating area changed from expansion to contraction, and permanent plastic deformation took place to the reverse direction. Finally, the free end of the tube bent to the direction toward to the laser beam. As shown in Fig. 10, the last deformation was 0.21 mm, while the bending angle can be calculated out as 0.48°.

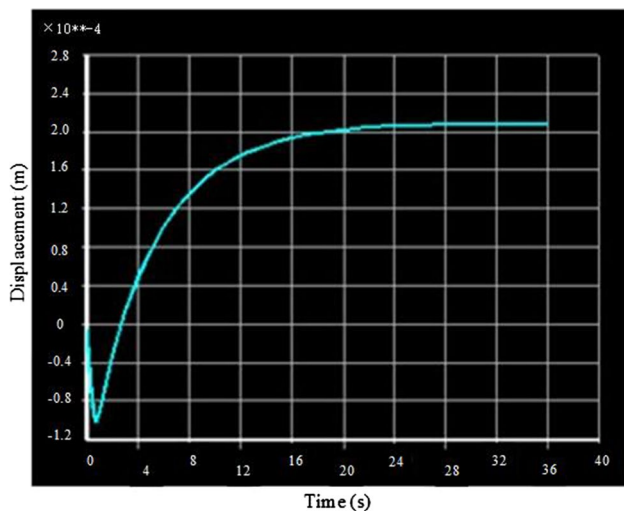


Fig. 10 Displacement of the free end in radial direction

**Table 3** Experiment data after single scan

Defomation of the free end (mm)	Bending angle (°)
Experiment data	
0.18	0.41
0.21	0.48
0.23	0.53
0.19	0.44
0.22	0.50
Average value	
0.206	0.47

## 3.2 Results of Bending Experiment

### 3.2.1 Deformation and Bending Angle After Single Scan

5 stainless steel tubes were scanned by the laser beam one time with processing parameters listed in Table 2. Deformations of the free end were measured using micrometer after each laser scanning. Then, the bending angles were calculated out, shown in Table 3.

Based on the result shown in Table 3, the error of the bending angle between FEM simulation and experiments were 2.08%. The error may induced by loading difference and absorption coefficient of the experimental tubes with coating.

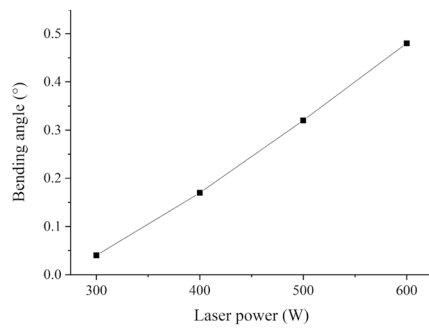
### 3.2.2 The Relationship Between the Bending Angle and Processing Parameters

The stainless steel tubes was scanned with the laser beam under different conditions and the change of the bending angle was recorded. Then, the relationships between the bending angle and the main parameters, such as laser power, scanning speed, spot diameter, and scanning times, were analyzed. The curves of the relationships are shown in Fig. 11.

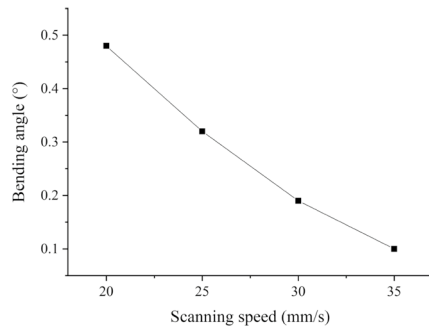
Figure 11a shows the effect of laser power on bending angle. It can be seen from the figure that the bending angle increased with the increase of laser power when the other conditions remained unchanged. The reason is that when the laser power increases, the heat flux loaded on the tube increases too. The tube absorbs more energy per unit of time and expands more so it endures larger compressive stress from the surrounding material and has greater plastic deformation when it is cooled. As a result, the bending angle is greater. The relationship is not linear and when the laser power is higher than 630 W, the tube cannot bend normally because the temperature is close to the melting point (1751 K) of the material, which is shown in Table 1.

Figure 11b is the relationship between the bending angle and scanning speed, which is along circumferential

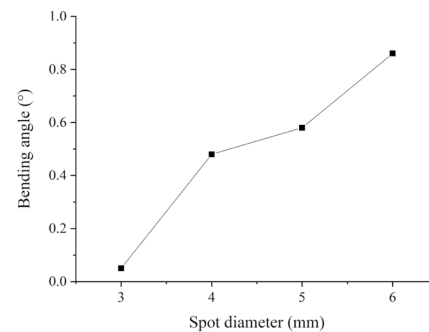




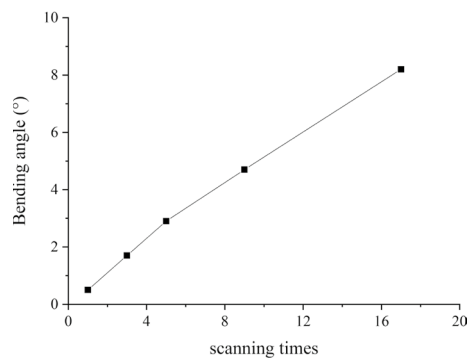
(a) Effect of laser power on bending angle (spot diameter 4 mm, rotation scanning speed 20 mm/s, scanning wrap angle 180°)



(b) Effect of scanning speed on bending angle (laser power 600W, spot diameter 4 mm, scanning wrap angle 180°)



(c) Effect of spot diameter on bending angle (laser power 600W, scanning speed 20 mm/s, scanning wrap angle 180°)



(d) Effect of scanning times on bending angle (laser power 600W, scanning speed 20 mm/s, spot diameter 4 mm, scanning wrap angle 180°)

Fig. 11 The effects of typical processing parameters on bending angle

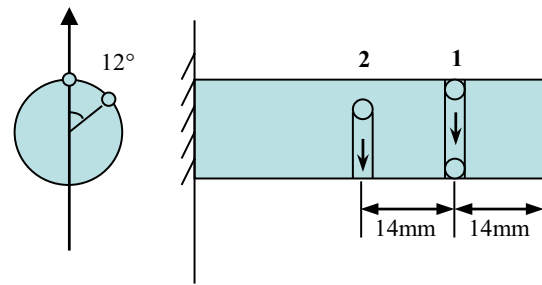


Fig. 12 Position of the scanning trajectory

direction. As is shown in the graph, the bending angle decreased with the increase of scanning speed (in a certain range) when the other conditions remained unchanged. With faster speed, the tube absorbed less energy, reached a lower temperature, and expanded less. As a result, the bending angle was smaller. The speed must be in the range from 17.5 to 35 mm/s because when the speed is lower than 17.5 mm/s, the highest temperature will be 1700 K and the tube will melt. When the speed is higher than 35 mm/s, the tube absorbs less energy and the bending angle is close to 0°.

Figure 11c shows the relationship between the bending angle and spot diameter with the same heat flux. It can be seen from the graph that the bending angle increased with the increase of the spot diameter when other conditions remained unchanged. With larger diameter, the tube absorbed more energy, expanded more, and produced larger plastic deformation. The spot diameter should be in a certain range, for the tube will not bend when the diameter is too small, and the bending direction and angle may be out of control when the diameter is too large [7].

Figure 11d shows the relationship of the bending angle and the scanning times. It can be seen in the graph that the bending angle increased with the increase of the scanning times. The bending angle was 0.42° after one scan and 8° after 16 scans.

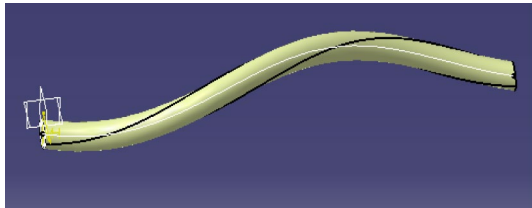
Thus, we can choose the appropriate number of times to scan to achieve the bending angle needed.

### 3.3 Result Based on Path Planning

To validate the path planning strategy described above, laser scanning experiments were conducted. The desired thread diameter was 20 mm and the desired pitch was 180 mm. The length of the tube was 230 mm. The target thread was divided into 15 sections and the axial offset of adjacent paths was 14 mm. According to Eqs. (6) and (7),  $\alpha$  was 18° and  $\beta$  was 12°. According to the relationship between bending angle and scanning times shown in Fig. 11, each path needed to be scanned 30 times. After



(a) Thread form tube produced in experiment



(b) Target shape of the thread form

**Fig. 13** Comparison of thread form tube produced in experiment with the target thread form

the completion of one path, the tube was rotated along the scanning direction for  $12^\circ$  as shown in Fig. 12.

Figure 13a shows the bending tube produced in the experiment. Its thread diameter was 20.6 mm and its thread pitch was 184.5 mm. Figure 13b shows the target shape of the tube. The errors of thread diameter and thread pitch were 3% and 2.5% respectively, which are both in an acceptable range. Therefore, it can be concluded that the desired thread form tube can be achieved with the proposed path planning strategy and method of optimizing the scanning parameters.

## 4 Conclusions

An indirect coupling analysis method based on ANSYS was carried out to study the mechanism of laser bending by analyzing the changing laws of temperature, stress, strain, and deformation in the bending process. The relationship between the bending angle and process parameters (laser power, scanning speed, spot diameter, and scanning time) was experimentally investigated using a  $\text{CO}_2$  laser and an NC supporting table. A path planning strategy for thread form bending of the tube was proposed by designing optimal scanning position, scanning route, scanning parameters. Finally, the strategy was verified by carrying out an experiment with a stainless steel tube. The dimension errors of the thread were in an acceptable range (3% for thread diameter

and 2.5% for thread pitch), which indicates the validity of the path planning strategy.

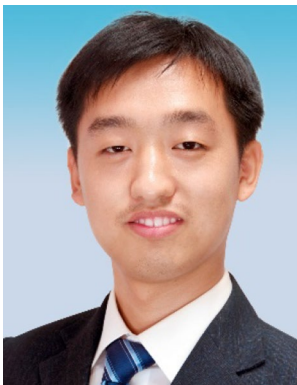
**Acknowledgements** This Project is funded by the Priority Academic Program Development of Jiangsu Higher Education Institutions. Fuqiang Li gives his deepest gratitude to Prof. Shourong Liu for enlightening and inspiring him towards this work.

## References

1. Yang, H., Li, H., Zhang, Z., Zhan, M., Liu, J., & Li, G. (2012). Advances and trends on tube bending forming technologies. *Chinese Journal of Aeronautics*, 25(1), 1–12.
2. Zhao, Z., Yang, H., Lin, Y., & Zhan, M. (2002). State of the art of the bending process and research of tube. *Metal Forming Technology*, 20(2), 1–5.
3. Zhan, M., Yang, H., & Jiang, Z. (2004). State of the art of research on tube bending process. *Mechanical Science and Technology*, 23(12), 1509–1514.
4. Yang, J. B., Jeon, B. H., & Oh, S. I. (2001). The tube bending technology of a hydroforming process for an automotive part. *Journal of Materials Processing Technology*, 111, 175–181.
5. Liu, S. H., Fang, X., & Fan, X. R. (2004). Experiment investigation on rules of laser tube bending. *Laser Technology*, 28(4), 340–343.
6. Akinlabi, S., & Akinlabi, E. (2018). Laser beam forming: A sustainable manufacturing process. *Procedia Manufacturing*, 21, 76–83.
7. Guan, Y., Sun, S., Zhao, G., & Yuan, G. (2006). Study on influence of process parameters on laser tube bending. *China Mechanical Engineering*, 17(S2), 1–4.
8. Silve, S., Steen, W. M., & Podschies, B. (1998). Laser forming tubes: A discussion of principles. In *Proceedings of ICALEO, section E* (pp. 151–160).
9. Kraus, J. (1997). Basic process in laser bending of extrusion using the upsetting mechanism. In *Laser assisted net shape engineering 2, proceedings of LANE*, vol. 2 (pp. 431–438). Germany: Meisenbach Bamberg.
10. Li, W., & Yao, Y. L. (2001). Laser bending of tubes: Mechanism, analysis, and prediction. *Journal of Manufacturing Science and Engineering*, 123(4), 674–681.
11. Hao, N., & Li, L. (2003). An analytical model for laser tube bending. *Applied Surface Science*, 208(1), 432–436.
12. Hao, N. H. (2007). Analysis of laser tube bending. *Journal of Plasticity Engineering*, 14(4), 40–43.
13. Safdar, S., Li, L., Sheikh, M. A., & Liu, Z. (2007). Finite element simulation of laser tube bending: Effect of scanning schemes on bending angle, distortions and stress distribution. *Optics & Laser Technology*, 39(6), 1101–1110.
14. Guan, Y., Yuan, G., Sun, S., & Zhao, G. (2013). Process simulation and optimization of laser tube bending. *The International Journal of Advanced Manufacturing Technology*, 65, 333–342.
15. Wang, X. Y., Luo, Y. H., Wang, J., Xu, W. J., & Guo, D. M. (2013). Scanning path planning for laser bending of straight tube into coil-shape tube. *The International Journal of Advanced Manufacturing Technology*, 69, 909–917.
16. Wang, X. Y., Wang, J., Xu, W. J., & Guo, D. M. (2014). Scanning path planning for laser bending of straight tube into curve tube. *Optics & Laser Technology*, 56, 43–51.

17. Imhan, K. I., Baharudin, B. T. H. T., Zakaria, A., Ismail, M. I. S. B., Alsabti, N. M. H., & Ahmad, A. K. (2017). Investigation of material specifications changes during laser tube bending and its influence on the modification and optimization of analytical modeling. *Optics & Laser Technology*, 95, 151–156.
18. Imhan, K. I., Baharudin, B. T. H. T., Zakaria, A., Alsabti, N. M. H., & Ahmad, A. K. (2017). An analytical and experimental investigation of average laser power and angular scanning speed effects on laser tube bending process. *MATEC Web of Conferences*, 95, 05008.
19. Imhan, K. I., Baharudin, B. T. H. T., Zakaria, A., Ismail, M. I. S. B., Alsabti, N. M. H., & Ahmad, A. K. (2018). Improve the material absorption of light and enhance the laser tube bending process utilizing laser softening heat treatment. *Optics & Laser Technology*, 99, 15–18.
20. Peckner, D., Bernstein, I. M., Gu, S., & Zhou, Y. (1987). *Handbook of stainless steels* (pp. 711–802). Beijing: China Machine Press.
21. Hao, N., & Pan, S. (2010). On the laser continuous bending of helical tube. *Journal of Beijing Information Science and Technology University*, 25(3), 9–13.

**Publisher's Note** Springer Nature remains neutral with regard to jurisdictional claims in published maps and institutional affiliations.



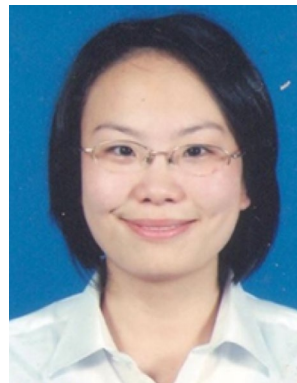
**Fuqiang Li** received his B.S. degree from Shandong University of Technology in 2010. And he received his Ph.D. degree in fatigue theory and reliability design from China Agricultural University in 2016. Now he works as a postdoctoral fellow in Institute of Agricultural Engineering, Jiangsu University, Zhenjiang, China. His current research interests include laser forming, agricultural engineering, electric tractor, fatigue reliability theory, energy control and management system, etc.



**Shourong Liu** received his Ph.D. degree from Jilin University of Technology in 1998. And he finished his postdoctoral research from Chiba University majored in material processing. Now he is a professor in China Agricultural University for 18 years, keeping studying on mechanical design, numerical simulation of manufacturing technology, lean manufacturing process, etc.



**Aiping Shi** received his B.S. degree from Jiangsu University in 1991. And he received his master's degree from Jiangsu University in 2007. Now he is a professor in Institute of Agricultural Engineering, Jiangsu University, Zhenjiang, China. His current research interests include tractor design, mechanical processing, comprehensive utilization of new energy, etc.



**Qiulu Chu** received her B.S. degree and Ph.D. degree from Nanjing Forestry University. She worked as Visiting Scholar and Postdoctoral Fellow in the University of British Columbia, Vancouver, Canada. Now she is an Associate Professor of Jiangsu University, Zhenjiang, China. Her current research interests include chemical processing engineering of forest and agriculture products, agricultural engineering, etc.



**Qiang Shi** received his bachelor's degree from Shandong university in 2009 and his master's degree from Shandong university in 2012. In 2013, he entered the school of agricultural equipment engineering, jiangsu university, working in the field of intelligent agricultural equipment.



**Yuxiang Li** received his bachelor's degree from Hangzhoudianzi University in 2015. And he received his Master degree from JiangSu University in 2018. His current research interests include agricultural engineering, electric tractor, motor control and fault diagnosis, etc.